Reduced phase error through optimized control of a superconducting qubit

Erik Lucero,[1] Julian Kelly,[1] Radoslaw C. Bialczak,[1] Mike Lenander,[1] Matteo Mariantoni,[1] Matthew Neeley,[1] A. D. O'Connell,[1] Daniel Sank,[1] H. Wang,[1] Martin Weides,[1] James Wenner,[1] Tsuyoshi Yamamoto,[1,2] A. N. Cleland,[1] and John M. Martinis[1,*]

[1]*Department of Physics, Broida Hall, University of California at Santa Barbara, Santa Barbara, California 93106, USA*

[2]*Green Innovation Research Laboratories, NEC Corporation, Tsukuba, Ibaraki 305-8501, Japan*

(Received 9 July 2010; published 29 October 2010)

Minimizing phase and other errors in experimental quantum gates allows higher fidelity quantum processing. To quantify and correct for phase errors, in particular, we have developed an experimental metrology—amplified phase error (APE) pulses—that amplifies and helps identify phase errors in general multilevel qubit architectures. In order to correct for both phase and amplitude errors specific to virtual transitions and leakage outside of the qubit manifold, we implement "half derivative," an experimental simplification of derivative reduction by adiabatic gate (DRAG) control theory. The phase errors are lowered by about a factor of five using this method to $\sim 1.6^\circ$ per gate, and can be tuned to zero. Leakage outside the qubit manifold, to the qubit $|2\rangle$ state, is also reduced to $\sim 10^{-4}$ for 20% faster gates.

DOI: 10.1103/PhysRevA.82.042339 PACS number(s): 03.67.Pp, 03.67.Ac, 03.67.Lx, 85.25.Cp

I. INTRODUCTION

Many candidate systems for quantum computation display several quantum energy levels, with computing architectures either employing just two of these levels [1–12], or using three or more in ("*d*-level") *qudit*-based approaches [2,6,13]. Achieving good control over the computational states, while avoiding interference from the noncomputational ones, requires measuring and understanding the source and magnitude of error-generating processes as well as correcting for such errors. For example, gate operations in the superconducting phase [2] and transmon [6] qubits, which are relatively weakly anharmonic, can generate leakage from the computational manifold to higher (noncomputational) levels ("manifold leakage"). However, by careful experimental design one can identify and minimize the source of such errors, thereby improving qubit control.

Previous experiments identified the amplitude errors associated with manifold leakage by using error budgeting and metrology [14]. By directly measuring leakage using the Ramsey error-filter protocol, this error is now understood and can be suppressed to $\sim 10^{-4}$ [14], at or near the threshold for fault-tolerant quantum computing [15,16]. Randomized benchmarking, an alternative approach to measuring gate error, relies on a many-pulse protocol, effectively averaging over the Bloch sphere to quantify gate fidelity [16,17]. Unfortunately, this approach optimizes a single value (gate fidelity) and does not distinguish between amplitude and phase errors. Quantum process tomography by contrast provides a complete analysis of gate operation [1,18,19], but requires calibrated $X_{\pi/2}$ and $Y_{\pi/2}$ pulses, which can themselves be error sources.

Phase errors also contribute to overall gate error, but the relative contribution differs from amplitude-related errors. Consequently, a method is needed to separately quantify the phase error generated by a gate. This will aid in identifying the source of these errors, improve calibration of high-fidelity tomography pulses, and provide a benchmark for optimizing control pulses.

In this paper we explicitly show that gate errors can be separated into amplitude and phase errors. Virtual excitations to noncomputational levels (e.g., the $|2\rangle$ state) during gate operation result in phase errors, while real excitations after the gate produce amplitude errors. In order to better quantify the phase errors, we introduce a metrology, "amplified phase error" (APE) pulses, which uses a Ramsey fringe experiment to measure and amplify this ubiquitous source of error. We focus on errors related to $\pi/2$ pulses, because such pulses provide the basis for tomography and are essential in algorithms. We also demonstrate a simplified experimental version of the protocol [20] termed "derivative removal by adiabatic gates" (DRAG) [15], which we call "half-derivative" (HD) pulses. By using HD pulses together with APE metrology, we measure and reduce the phase error to 1.6° per gate, a factor of five reduction from unoptimized performance. As a demonstration of this method, we perform quantum state tomography to map out the trajectories of typical HD pulses, including a π pulse and a rotation about an arbitrary axis, using X, Y, and Z controls to implement an (off-equator) Hadamard gate. In addition, we show that APE metrology is a universal tool for probing phase errors on any of the higher qudit levels.

II. QUBIT CONTROL

In the experiments described here, we used a single superconducting phase qubit with $T_1 = 450$ ns and $T_2^{\text{echo}} = 390$ ns. The circuit layout and operation have been described previously [2]. We have three-axis control over the qubit: Microwave pulses of arbitrary amplitude and phase, resonant with the qubit $|1\rangle \leftrightarrow |0\rangle$ transition frequency f_{10}, produce rotations about any axis in the x-y plane, while current pulses on the qubit bias line adiabatically change the qubit frequency, causing phase accumulation between $|0\rangle$ and $|1\rangle$, generating z-axis rotations [21]. The $|2\rangle \leftrightarrow |1\rangle$ transition frequency f_{21} differs from f_{10} by $\Delta/2\pi = f_{21} - f_{10} \sim -200$ MHz.

Nonideal qubit behavior can arise from both leakage at the end of the gate and virtual transitions to higher states during on-resonant operations. The leakage is an amplitude error, representing loss of probability to states outside the manifold. Leakage can be reduced to $\sim 10^{-4}$ by careful shaping of the

*martinis@physics.ucsb.edu

microwave envelope and choosing the correct gate duration, which scales as $1/\Delta$ [14,22].

III. PHASE ERROR

The phase error arising from virtual transitions (especially to the $|2\rangle$ state) can be modeled as effective qubit rotations about the z axis. We first restrict ourselves to simple gates comprising π and $\pi/2$ rotations. An $X_{\pi/2}$ pulse (a rotation about the x axis by an angle $\theta = \pi/2$) ideally produces the transformation,

$$X_{\pi/2} = e^{-i\sigma_x \frac{\pi}{4}} = \frac{1}{\sqrt{2}} \begin{pmatrix} 1 & -i \\ -i & 1 \end{pmatrix}, \tag{1}$$

where σ_x is one of the Pauli matrices. From numerical simulations of our multilevel qubit, we find that this transformation, expressed in quantum circuit language, is instead

$$X'_{\pi/2} = e^{-i\epsilon'} Z_\epsilon X_{\pi/2} Z_\epsilon, \tag{2}$$

where Z_ϵ is the phase error of interest and $0 < \epsilon \ll 1$ (see Appendix B). The leading term in Eq. (2) is a global phase and can be ignored. We note that Eq. (2) differs from $X^\star_{\pi/2} = Z_{-\epsilon} X_{\pi/2} Z_\epsilon$, which corresponds to a rotation about a new axis ϵ away from the x axis in the x-y plane.

The phase error ϵ is a function of both the rotation angle θ and the gate time t_g. From simulations, we find that $\epsilon \sim \theta^2/t_g$. Longer gate times decrease the virtual transitions and consequently reduce the phase error, consistent with the ac-Stark effect [23].

A. Amplifying phase error

In order to best reduce this error, we first sought a protocol that would amplify the error ϵ (see Appendix B). If we consider a 2π rotation generated by concatenating four $\pi/2$ pulses, we find from Eq. (2) that $X'^4_{\pi/2} = -e^{-4i\epsilon'} I$, where I is the identity (see Appendix B). A concatenated 2π rotation thus does not accumulate the relative phase error.

We next examine the pseudoidentity operation that is formed by concatenating positive and negative θ rotations. For a first-order expansion with $\epsilon \ll 1$ we find

$$\begin{aligned} I'_\theta &= (Z_\epsilon X_\theta Z_\epsilon)(Z_\epsilon X_{-\theta} Z_\epsilon) \\ &\approx \begin{pmatrix} 1 + i(\cos\theta - 1)\epsilon & -(\sin\theta)\epsilon \\ (\sin\theta)\epsilon & 1 - i(\cos\theta + 3)\epsilon \end{pmatrix}, \end{aligned} \tag{3}$$

where X_θ is an arbitrary rotation of θ about the x axis (see Appendix B). For $\theta = \pi$ we find that $I'_\pi = e^{-2i\epsilon'} I$, which is similar to the 2π rotation, as the phase error ϵ cancels. However, for $\theta = \pi/2$ we find

$$\begin{aligned} I'_{\pi/2} &= (Z_\epsilon X_{-\pi/2} Z_\epsilon)(Z_\epsilon X_{\pi/2} Z_\epsilon) \\ &\approx \begin{pmatrix} 1 - i\epsilon & \epsilon \\ -\epsilon & 1 - 3i\epsilon \end{pmatrix}, \end{aligned} \tag{4}$$

showing phase error accumulation.

B. Measuring phase error

To measure this error, we combine the result from Eq. (4) with a Ramsey fringe experiment, forming the "amplified phase error" (APE) sequence. The APE sequence consists of inserting n successive $I'_{\pi/2}$ pseudoidentity operations between the $\pi/2$ pulses that define a Ramsey fringe measurement [Fig. 1(b)]. The phase error is amplified by $2n$ for n applications of the pseudoidentity operation,

$$I'^n_{\pi/2} \approx (Z_{2\epsilon})^n = Z_{2n\epsilon}. \tag{5}$$

By applying APE pulses to the state $|\psi\rangle = (|0\rangle - i|1\rangle)/\sqrt{2}$ followed by a final $\phi_{\pi/2}$ pulse, we directly probe the phase error due to the $X_{\pi/2}$ pulses.

Figure 1(b) shows the probability of measuring the $|1\rangle$ state versus rotation axis ϕ of the final $\phi_{\pi/2}$ pulse for $I'^n_{\pi/2}$ ($n = 0$, 1,3,5) pseudoidentity operations. Consistent with Eq. (5), the phase error scales with n. For $n = 5$ in Fig. 1(b), the final pulse is 83° out of phase, corresponding to a 10× phase error amplification from a total of 11 pulses (10 from the APE sequence and 1 from the initial $X_{\pi/2}$), yielding a 7.3° phase error per gate (see Fig. 6). The oscillation amplitude is also reduced, due to decoherence.

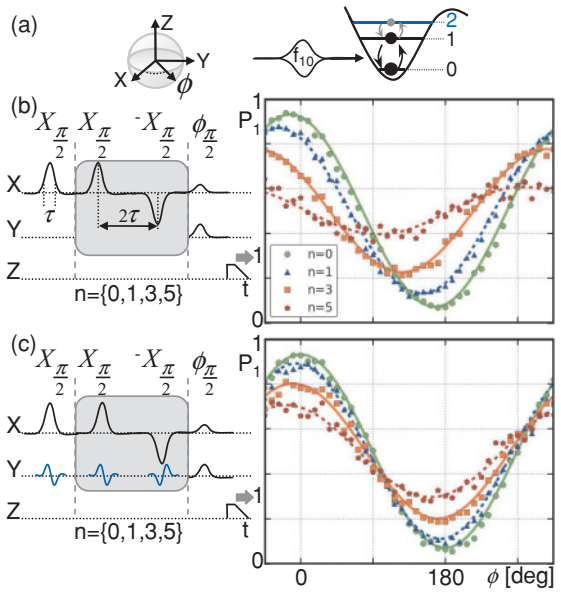

FIG. 1. (Color online) Multilevel qubit and amplified phase error (APE) metrology. (a) Bloch sphere indicating the axes of rotations and a qubit with three energy levels, illustrating phase error due to virtual transitions to the $|2\rangle$ state. While performing on-resonance $|0\rangle \leftrightarrow |1\rangle$ gate operations at frequency f_{10}, virtual transitions to $|2\rangle$ create a phase change in $|1\rangle$. (b) (Left) Single-control (X-quadrature) APE pulse sequence, where the pulse shape represents the microwave envelope, with τ denoting the full width at half maximum (FWHM). All control pulses are separated in time by 2τ. Ramsey-fringe experiments are modified by $I'^n_{\pi/2}$ ($n \in \{0,1,3,5\}$) pseudoidentity operations in between the first $X_{\pi/2}$ and last $\phi_{\pi/2}$ pulses. At the end the Z control line is pulsed to measure the probability of $|1\rangle$. (Right) The probability of measuring $|1\rangle$ as a function of the rotation axis ϕ of the final $\pi/2$ pulse; each data point is repeated 1200 times. Fits to extract the phase shift are plotted as lines with the data (dots). (c) (Left) Same pulse sequence as in (a), but with the addition of Y-quadrature "half-derivative" pulses, as discussed in the text. (Right) The data (dots) with fits (lines) show small phase shifts for the HD pulse sequence.

C. Correcting phase error

To correct the phase error, we employ the derivative reduction by adiabatic gates (DRAG) protocol [15]. The original DRAG prescription uses three controls, X, Y, and Z. The X control provides the original envelope shaping to the microwaves, which we implemented as a Gaussian in time with arbitrary amplitude A, $X = A\exp[-4\ln(2)(t-t_0)^2/\tau^2]$, where τ is the full width at half maximum (FWHM) and t_0 the time at the center of the pulse. The quadrature control $Y = -\dot{X}/\Delta$ is the time derivative of the X control scaled by the nonlinearity Δ. The Z control produces a dynamic detuning pulse during the gate that removes the effective z rotations from the virtual transitions.

We find both in simulations and experiment that the Y and Z controls are not independent (see Appendix C). For experimental simplicity, we set Z to zero and compensate by reducing the magnitude of the Y control by 1/2, to form the so-called "half-derivative" (HD) protocol. For a Gaussian envelope on the X control, the HD pulses are as illustrated in Fig. 1(c) and differ from the DRAG pulses by the quadrature controls, $Y = -\dot{X}/(2\Delta)$, $Z = 0$.

The HD pulse sequence in Fig. 1(c) is the same as Fig. 1(b), with the addition of the Y control. Data are plotted for the same number of $I'_{\pi/2}$ pseudoidentity operations. We find by applying the HD protocol the phase error is reduced to 1.6° per gate, and can be further minimized by tuning the amplitude of the derivative pulse.

IV. AMPLITUDE ERROR

HD pulses also reduce the leakage to the $|2\rangle$ state. Plotted in Fig. 2 are the data from a Ramsey error filter [14] for both single-control Gaussian and HD pulses. A 6-ns (FWHM) HD X_π pulse gives a $|2\rangle$ state probability of 10^{-4}, almost an order of magnitude better than a non-HD pulse of the same width, which consequently provides a 20% faster gate [14].

V. DEMONSTRATING CONTROL

With calibrated $X_{\pi/2}$ and $Y_{\pi/2}$ pulses, we can perform quantum state tomography (QST) without worry of miscalibrated

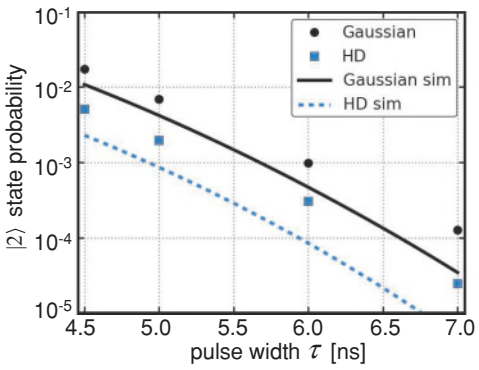

FIG. 2. (Color online) Amplitude errors due to leakage into the $|2\rangle$ state from an X_π pulse. Plot of $|2\rangle$ error versus pulse width (FWHM) τ for single-control Gaussian (black dots) and HD (blue squares) π pulses. The 6-ns HD pulse produces ×5 lower error and 20% faster gates. The lines are three-state simulations using Gaussian (solid black) and HD (dashed blue) pulses.

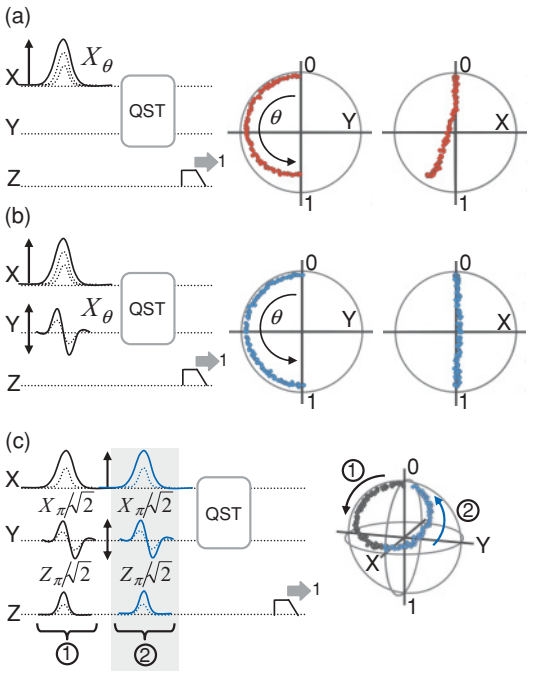

FIG. 3. (Color online) Gate trajectories using quantum state tomography (QST) for single-control and HD pulses. (a) (Left) Pulse sequence for an X rotation. A Gaussian pulse of fixed length (FWHM = 6 ns) and varying amplitude completes the rotation angle to $\theta = \pi$. QST is performed at every incremental increase of amplitude. (Right) The reconstructed quantum state data are plotted on the Bloch sphere from two perspectives, looking down the x and the $-y$ axes. (b) Same as in (a) except using HD (X and Y simultaneous control) pulses to perform the X rotation. No phase error is observed. (c) (Left) Pulse sequence of a two-part trajectory using HD pulses and Z control to form a Hadamard gate. X, Y, and Z controls are fixed-length (FWHM = 6 ns) pulses with increasing amplitudes to execute $\pi/\sqrt{2}$ rotations about X and Z. Trajectory 2 pulses ramp up only after trajectory 1 pulses are at full amplitude. (Right) The reconstructed QST data. Each trajectory completes a Hadamard gate, taking $|0\rangle \rightarrow (|0\rangle + |1\rangle)/\sqrt{2} \rightarrow |0\rangle$.

measurement axes. As a practical demonstration of how HD pulses reduce phase error, we perform QST [21] with and without HD. Figure 3(a), panel (b), shows the pulse sequence and data for the Gaussian pulses (HD pulses) during an X_θ rotation. The pulses are of fixed length (FWHM = 6 ns) with variable amplitude θ. QST is performed at each incremental increase of amplitude and the quantum state is recreated in the Bloch sphere as shown to the right of each of the respective pulse sequences. In contrast with the single control Gaussian pulses, the HD pulses execute a meridian trajectory with no phase error with increasing θ.

The final HD demonstration is an (off-equator) Hadamard gate, shown in Fig. 3(c), which uses all three control lines (see Appendix D). We incrementally increase the amplitude of all three control lines using fixed length (FWHM = 6 ns) pulses to perform rotations from 0 to $\pi/\sqrt{2}$ about both the x and z axes, which at full amplitude gives the Hadamard gate H $[|0\rangle \rightarrow (|0\rangle + |1\rangle)/\sqrt{2}]$. The trajectory concludes with a second set of pulses to complete the identity operation $I = HH$, and returning to the initial state $(|0\rangle + |1\rangle)/\sqrt{2} \rightarrow |0\rangle$.

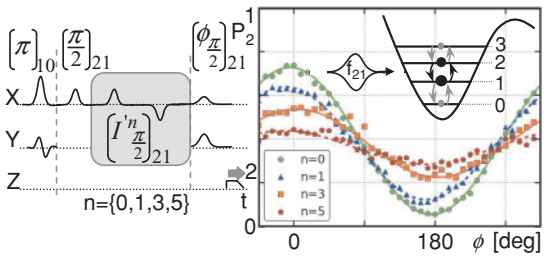

FIG. 4. (Color online) Multilevel qudit and APE metrology for the $|1\rangle \leftrightarrow |2\rangle$ transition. (Inset) The four energy levels of the qudit illustrate the nearly symmetric virtual transitions to states $|3\rangle$ and $|0\rangle$ that mostly cancel the phase error during the f_{21} resonant drive. (Left) Pulse sequence showing $(\pi)_{10}$ for a $|0\rangle \rightarrow |1\rangle$ transition then a Ramsey fringe with the pseudoidentity operation on the $|1\rangle \leftrightarrow |2\rangle$ transition. (Right) The probability of measuring the $|2\rangle$ state as a function of the rotation axis of the final $(\phi_{\pi/2})_{21}$ pulse for $n \in \{0,1,3,5\}$ pseudoidentity operations. With only a single-control pulse (no HD correction), the phase error is 1.1° per gate.

VI. AMPLIFIED PHASE ERROR FOR HIGHER LEVELS

We also consider the challenge of optimizing control pulses for each d level of a qudit [2]. Tomography verifies the operation, but again relies on the calibrations of $\pi/2$ pulses. In principle, APE provides the necessary phase calibration certification for tomography.

To demonstrate the general utility of the APE protocol, we implement this metrology on the qudit level for state $|2\rangle$. We first calibrate the $(\pi)_{10}$ and $(\pi)_{21}$ pulses to generate the $|0\rangle \rightarrow |1\rangle$ and $|1\rangle \rightarrow |2\rangle$ transitions, respectively [2]. As shown in Fig. 4, we first prepare the $|1\rangle$ state via an HD π pulse so that we can then perform a Ramsey fringe experiment using the $|1\rangle$ and $|2\rangle$ states. The APE pulses are applied between the first and last $(\pi/2)_{21}$ pulses, only now resonant with f_{21}. The data are for single-controlled Gaussian envelope pulses (i.e., no HD protocol for the $|1\rangle \rightarrow |2\rangle$ pulses).

Surprisingly, after $n = 5$ pseudoidentity operations, only 12° of phase error is measured, equivalent to 1.1° per gate. We offer a qualitative interpretation: the relatively small anharmonicity of the phase qudit, combined with the symmetric virtual transitions to the $|3\rangle$ and $|0\rangle$ states, provide complementary phase shifts that partially cancel out the phase error.

VII. CONCLUSION

In conclusion, we introduced a metrology tool, amplified phase error (APE) pulses, which can amplify the phase error by an order of magnitude. Together with APE and half-derivative pulses, our simplified variant of DRAG [15], we identify and reduce phase errors to 1.6° per gate. By simply rescaling the analytic form for the HD pulses, the phase error can be completely removed. The HD pulses also can increase gate speed by 20%.

ACKNOWLEDGMENTS

We acknowledge discussions with Jerry Chow, Jay Gambetta, Felix Motzoi, and Frank Wilhelm. Devices were made at the University of California at Santa Barbara Nanofabrication Facility, part of the National Nanotechnology Infrastructure Network, funded by the National Science Foundation. M.M. acknowledges the support from the Elings Foundation. This work was supported by Intelligence Advanced Research Projects Activity under Grant No. W911NF-04-1-02-4.

APPENDIX A: TRACKING QUBIT FREQUENCY

Optimized qubit control pulses rely on a precise measurement of the qubit transition frequency. After performing spectroscopy to find the qubit frequency f_{10} to within ~1 MHz, we fix the gate time τ and tune the microwave amplitude to execute a π rotation. We verify that the computed amplitude for $\pi/2$ rotation is indeed half that for a π rotation by performing two consecutive $\pi/2$ rotations and comparing the probability P_1 between that of a single π rotation.

Next, to precisely measure the qubit frequency, we use a Ramsey fringe experiment, where the final $\phi_{\pi/2}$ pulse rotates at 50 MHz about a variable axis on the equator of the Bloch sphere. A frequency shift in the oscillations of P_1 different from 50 MHz is the amount the microwave drive is detuned from the qubit frequency. Correcting for this offset precisely tunes the microwave drive to the qubit frequency to within 1 part in 10^4 (sub-MHz resolution), which is consistent with limits set from $1/f$ flux-noise fluctuations [24].

We also can perform a more complete test [two-dimensional (2D) scans] of this frequency calibration by noting that the phase error is $\epsilon = \delta f \delta t$ if the microwave drive is δf off resonance from the qubit frequency for some time δt. Therefore, we verify that the microwave carrier matches the qubit frequency for the entire δt of the APE sequences via a Ramsey fringe experiment as shown in Fig. 5. Figure 5(b) shows the data for two different detunings: (left) $\delta f = 10$ MHz and (right) $\delta f < 1$ MHz (after performing the calibration described previously). When the microwave drive is detuned by $\delta = 10$ MHz the data show a distinct tilt and clear oscillations with a frequency of 10 MHz. After calibration the data have no

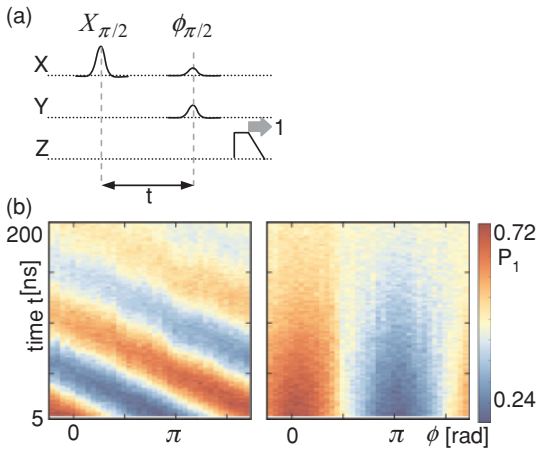

FIG. 5. (Color online) Tracking the qubit frequency f_{10}. (a) Ramsey fringe sequence that consists of two Gaussian-shaped $\pi/2$ pulses, separated in time by t, followed by a measure pulse on the Z control tuned to tunnel the $|1\rangle$ state. The first $\pi/2$ pulse defines the rotation axis; by convention this is the x axis. The second pulse is delayed by a time t with variable rotation axis ϕ. (b) Plots of P_1 versus separation time t and phase ϕ for pulse sequence in (a). (Left) Microwave drive is 10 MHz detuned from the qubit frequency f_{10}. (Right) Data taken after calibration; microwaves detuned less than 1 MHz from the qubit frequency.

beating and therefore no sign of a detuned microwave drive. This confirms that the qubit frequency is tracked precisely throughout the duration of the desired (amplified phase error) sequences. We note that the APE sequences are shorter than the dephasing time.

To compute the nonlinearity $\Delta/2\pi = f_{21} - f_{10}$ for use in the HD protocol, we directly measure the transition frequency between states $|1\rangle$ and $|2\rangle$ with a Ramsey error filter (REF) [14]. The REF uses an oscillation, provides finer resolution, and is simpler to automate experimentally than for peak finding in high-power spectroscopy. To increase the $|2\rangle$ state population, the $(\pi)_{10}$ pulses (for the $|0\rangle \leftrightarrow |1\rangle$ transitions) are sufficiently short and do not use the HD protocol. Using this technique, we measure the $|1\rangle \rightarrow |2\rangle$ transition frequency, f_{21} to within 1 MHz.

APPENDIX B: AMPLIFIED PHASE ERROR THEORY

Our numerical simulations are for a three-level system with qubit parameters and nonlinearity corresponding to experimental conditions. We use integration of the Schrödinger equation to explicitly calculate the time evolution for an arbitrary input state, which is described by a 3×3 unitary matrix U. With an appropriate Gaussian control pulse, we find the elements of U that connect the $|0\rangle$ or $|1\rangle$ state with the $|2\rangle$ state have small magnitude, consistent with the negligible $|2\rangle$ state error as reported previously [14]. The time evolution of the two qubit states is thus well described by the 2×2 submatrix of U. We find that for small phase errors, this submatrix can be written as

$$X'_{\pi/2} \simeq Z_\epsilon X_{\pi/2} Z_\epsilon, \tag{B1}$$

where Z_ϵ is the phase error of interest,

$$Z_\epsilon = \begin{pmatrix} 1 & 0 \\ 0 & e^{-i\epsilon} \end{pmatrix}. \tag{B2}$$

Moreover, from these simulations, with control pulses of length 6 ns and typical nonlinearities $\Delta/(2\pi) = -200$ MHz, we plot in Fig. 6 the expected phase error versus rotation angle for an uncorrected Gaussian control pulse. Initially, the phase error increases parabolically, then saturates and decreases. Although the maximum occurs at an angle slightly larger than

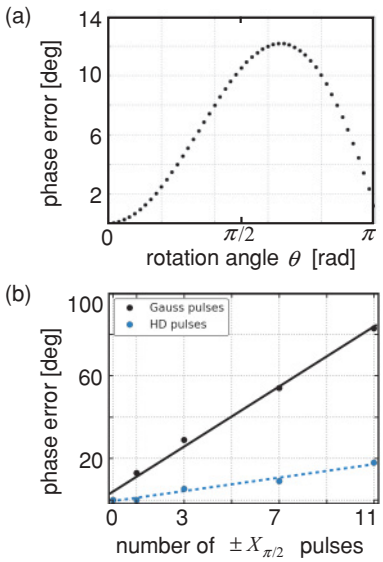

FIG. 6. Phase error per pulse from numerical simulations and APE experiments. (a) Numerical simulation for a three-level qubit starting in $|0\rangle$ and rotating by an angle $\theta = 0$ to π due to a Gaussian control pulse. The phase error versus rotation angle θ is plotted. (b) Amplified phase error data. Phase error versus number of $\pm X_{\pi/2}$ pulses is plotted with lines as fits to extract the phase error per pulse for both Gaussian (solid black) and HD (dashed blue) pulses.

$\pi/2$, $\pi/2$ pulses were chosen for their important role for tomography.

Using Eqs. (B1) and (B2), we explicitly calculate the phase shift for a 2π rotation coming from four $\pi/2$ pulses. For an arbitrary rotation θ about the x axis, the gate operation is

$$X_\theta = \begin{pmatrix} \cos\theta/2 & -i\sin\theta/2 \\ -i\sin\theta/2 & \cos\theta/2 \end{pmatrix}, \tag{B3}$$

such that $X'_{\pi/2}$ is

$$X'_{\pi/2} = \frac{1}{\sqrt{2}} \begin{pmatrix} 1 & -ie^{-i\epsilon} \\ -ie^{-i\epsilon} & e^{-i2\epsilon} \end{pmatrix}. \tag{B4}$$

Concatenating four positive $\pi/2$ rotations results in

$$X'^4_{\pi/2} \equiv (X'_{\pi/2})^4 = \frac{1}{4} \begin{pmatrix} e^{-6i\epsilon}(-1 - e^{2i\epsilon} - 3e^{4i\epsilon} + e^{i\epsilon}) & -ie^{-7i\epsilon}(-1 + e^{2i\epsilon})^2(1 + e^{2i\epsilon}) \\ -ie^{-7i\epsilon}(-1 + e^{2i\epsilon})^2(1 + e^{2i\epsilon}) & e^{-8i\epsilon}(-1 + 3e^{2i\epsilon} + e^{4i\epsilon} + e^{6i\epsilon}) \end{pmatrix} \simeq e^{-i4\epsilon} I, \tag{B5}$$

where I is the identity. Equation (B5) only acquires a global phase.

Next, we calculate the phase shift for the pseudoidentity operation, used in the APE protocol, comprising a positive then a negative $\theta = \pi/2$ rotation,

$$\begin{aligned} I'_{\pi/2} &= X'_{-\pi/2} X'_{\pi/2} \\ &= \begin{pmatrix} e^{-i\epsilon}\cos(\epsilon) & e^{-2i\epsilon}\sin(\epsilon) \\ -e^{-2i\epsilon}\sin(\epsilon) & e^{-3i\epsilon}\cos(\epsilon) \end{pmatrix} \\ &\approx \begin{pmatrix} 1 - i\epsilon & \epsilon \\ -\epsilon & 1 - 3i\epsilon \end{pmatrix}. \end{aligned} \tag{B6}$$

For n applications of the pseudoidentity operation, in the limit where $0 < \epsilon \ll 1$, $\epsilon \rightarrow n\epsilon$

$$I'^n_{\pi/2} \approx \begin{pmatrix} 1 - in\epsilon & n\epsilon \\ -n\epsilon & 1 - 3in\epsilon \end{pmatrix}, \tag{B7}$$

focusing on the relative phase along the diagonal elements, and by removing an overall global phase,

$$I'^n_{\pi/2} \approx (Z_{2\epsilon})^n = Z_{2n\epsilon}. \tag{B8}$$

The measured phase shift scales with the number n of pseudoidentity operations, or equivalently the number of applied $\pm X_{\pi/2}$ pulses, as shown in Fig. 6(b).

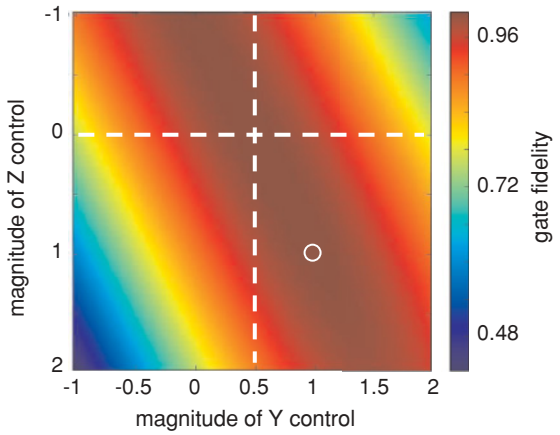

FIG. 7. (Color online) Numerical simulations of gate fidelity for a three-level system with $\Delta/(2\pi) = -200$ MHz. All simulated pulses are of the DRAG prescription and a fixed length of 6 ns. The white circle indicates the values, $Z = 1$ and $Y = 1$, as proposed in Ref. [15]. White dotted lines highlight the HD operating magnitudes.

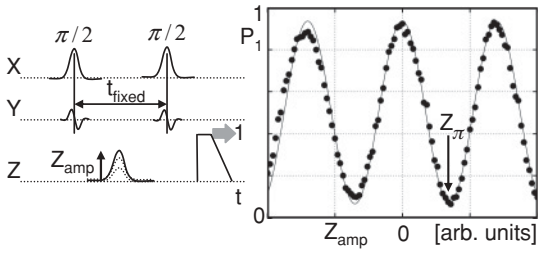

FIG. 8. Z_π calibration. (a) (Left) The Ramsey-type pulse sequence to calibrate a Z_π with the X and Y controls using the HD protocol described in the manuscript. The sequence consists of two, 6-ns (FWHM) $\pi/2$ pulses fixed in time with $t_{\text{fixed}} = 24$ ns and a 6-ns (FWHM) Z pulse centered in between them. The separation time is chosen to minimize overlap of the pulses. The Z_{amp} increases incrementally. (Right) The probability of measuring the $|1\rangle$ state P_1 as a function of Z-pulse amplitude, Z_{amp}. The data are plotted as points with best fit as a line. P_1 oscillates with increasing magnitude of the Z-pulse amplitude. The arrow indicates the Z-pulse amplitude equivalent to a π rotation about the Z axis.

APPENDIX C: HALF DERIVATIVE

From the numerical simulations described in Appendix C, we plot in Fig. 7 the gate fidelity defined as $F = \text{Tr}(\chi_{\text{sim}}\chi_{\text{ideal}})$ in a color scale for a range of magnitudes for the Y and Z controls. The circle in Fig. 7 indicates the values from the original DRAG prescription, $Y = 1$ and $Z = 1$ [15]. We find there is a ridge of maximum fidelity for the two control parameters, with peak values of fidelity having a simple linear relation between the Y and Z values. Along this ridge, the maximum fidelity is insensitive to Z. We set the Z control to zero, which simplifies the experimental control procedures as it reduces the necessary control signals for optimal pulses from 3 to 2.

The Y control provides a dynamic detuning to the qubit, which keeps the microwave drive and the qubit on resonance during the gate operation performed by the X control, similar to the role the Z control plays in the original DRAG prescription [15].

By simply using the analytic expression for HD, $Y = -\dot{X}/(2\Delta)$ we reduce the phase error to 1.6° per pulse. For higher phase sensitivity experiments one can utilize the APE experiment to tune the phase error to zero by adjusting the magnitude of the Y control.

APPENDIX D: Z-PULSE CALIBRATION

Explicit Z gates are required for the (off-equator) Hadamard gate. We calibrate our Z pulse as shown in Fig. 8. A static length (full width at half maximum = 6 ns) with an increasing amplitude Z pulse inserted between two HD $\pi/2$ pulses with fixed separation time t_{fixed}. The probability of measuring the $|1\rangle$ state P_1 oscillates with increasing Z_{amp} [21]. The arrow indicates the Z_{amp} that corresponds to a rotation angle of π about the z axis.

[1] M. A. Nielsen and I. L. Chuang, *Quantum Computation and Quantum Information* (Cambridge University Press, Cambridge, 2000).
[2] M. Neeley *et al.*, Science **325**, 722 (2009).
[3] J. I. Cirac and P. Zoller, Phys. Rev. Lett. **74**, 4091 (1995).
[4] N. A. Gershenfeld and I. L. Chuang, Science **275**, 350 (1997).
[5] R. Bianchetti, S. Flipp, M. Baur, J. M. Fink, C. Lang, L. Steffen, M. Boissonneault, A. Blais, and A. Wallraff, e-print arXiv:1004.5504v1.
[6] L. DiCarlo *et al.*, Nature (London) **460**, 240 (2009).
[7] J. Q. You and F. Nori, Phys. Today **58**, 42 (2005).
[8] A. Imamoglu, Phys. Rev. Lett. **102**, 083602 (2009).
[9] J. R. Weber, W. F. Koehl, J. B. Varley, A. Janotti, B. B. Buckley, C. G. Van de Walle, and D. D. Awschalom, Proc. Natl. Acad. Sci. USA **107**, 8513 (2010).
[10] P. M. Platzman and M. I. Dykman, Science **284**, 1967 (1999).
[11] J. R. Petta *et al.*, Science **309**, 2180 (2005).
[12] J. M. Martinis, S. Nam, J. Aumentado, and C. Urbina, Phys. Rev. Lett. **89**, 117901 (2002).
[13] T. Yamamoto *et al.*, e-print arXiv:1006.5084v1.
[14] E. Lucero, M. Hofheinz, M. Ansmann, R. C. Bialczak, N. Katz, M. Neeley, A. D. OConnell, H. Wang, A. N. Cleland, and J. M. Martinis, Phys. Rev. Lett. **100**, 247001 (2008).
[15] F. Motzoi, J. M. Gambetta, P. Rebentrost, and F. K. Wilhelm, Phys. Rev. Lett. **103**, 110501 (2009).
[16] E. Knill, Nature (London) **434**, 39 (2005).
[17] J. M. Chow, J. M. Gambetta, L. Tornberg, J. Koch, L. S. Bishop, A. A. Houck, B. R. Johnson, L. Frunzio, S. M. Girvin, and R. J. Schoelkopf, Phys. Rev. Lett. **102**, 090502 (2009).
[18] M. Neeley *et al.*, Nature Physics **4**, 523 (2008).
[19] R. C. Bialczak *et al.*, Nature Physics **6**, 409 (2010).

[20] J. M. Chow, L. DiCarlo, J. M. Gambetta, F. Motzoi, L. Frunzio, S. M. Girvin, and R. J. Schoelkopf, e-print arXiv:1005.1279v1.

[21] M. Steffen, M. Ansmann, R. McDermott, N. Katz, R. C. Bialczak, E. Lucero, M. Neeley, E. M. Weig, A. N. Cleland, and J. M. Martinis, Phys. Rev. Lett. **97**, 050502 (2006).

[22] M. Steffen, J. M. Martinis, and I. L. Chuang, Phys. Rev. B **68**, 224518 (2003).

[23] B. W. Shore, Phys. Rev. A **17**, 1739 (1978).

[24] R. C. Bialczak *et al.*, Phys. Rev. Lett. **99**, 187006 (2007).